PERGAMON

International Journal of Heat and Mass Transfer 43 (2000) 1209–1222

International Journal of HEAT and MASS TRANSFER

www.elsevier.com/locate/ijhmt

# Modelling of an electric IR heater at transient and steady state conditions Part I: model and validation

Magnus Pettersson*, Stig Stenström

*Department of Chemical Engineering 1, Lund University, P.O. Box 124, SE-221 00 Lund, Sweden*

Received 18 February 1999; received in revised form 14 May 1999

**Abstract**

A model for an electric infrared (IR) heater has been developed. The model includes non-grey radiative heat transfer between the different parts of the IR heater, as well as conduction in reflector material and convective cooling of surfaces. The geometry is simplified into one dimension. Using IR module voltage as the only input, the model predicts the temperature of heater components and cooling air, as well as the net radiation heat transfer to the surroundings at steady state and transient conditions. The model has been validated against both steady state and transient experimental results from a small electric IR heater. The model predictions are in good agreement with experimental data both regarding steady state results and the transient response over a wide range of voltages. 

*Keywords:* IR; Electric heater; Radiation heat transfer; Modelling; Measurements; Transients

## 1. Introduction

Infrared (IR) heaters are used in industry for heating and drying operations. Two different types of IR heaters dominate these applications, i.e., medium-wave gas-fired IR heaters and short-wave electric IR heaters. Gas-fired IR heaters have achieved some attention in the scientific literature, with papers presenting advanced modelling work [1–3] and experimental studies [4,5]. Fundamental studies on electric IR heaters are much more scarce. There are some publications that discuss experimental work [6–8] and work regarding radiation exchange modelling, especially the pioneering work in infrared paper drying by Lampinen, Ojala and co-workers [9,10]. These models are focused on radiation exchange and the interaction with paper. The temperatures of the different parts of the heater are given a priori and are considered as the result of cooling air system design. Pettersson and Stenström [11] developed a similar model in order to obtain a spectral distribution of radiation for their study on internal radiation transport in paper sheets. However, they did notice the limitation of not being able to include the effect of paper grade on the temperature of the different components in the IR dryer.

This work will propose a model for an electric IR heater. The model will be able to predict the temperature of the heater components under different operating conditions, as well as the transient behaviour during the start-up and close-down of the heater.

* Corresponding author. Tel.: +46-46-222-82-96; fax: +46-46-222-45-26.

*E-mail address:* Magnus.pettersson@kat.lth.se (M. Pettersson).

0017-9310/00/$ - see front matter 
PII: S0017-9310(99)00201-X

**Nomenclature**

| | |
|---|---|
| $A$ | area ($m^2$) |
| $a_f$ | filament cross section ($m^2$) |
| $c_0$ | speed of light, $2.998 \times 10^8$ (m/s) |
| $C_p$ | specific heat (J/kg K) |
| $d$ | diameter (m) |
| $E$ | blackbody emissive power ($W/m^2$) |
| $\varepsilon_{\lambda,i}$ | emissivity of surface $i$ at wavelength $\lambda$ |
| $f\langle x\rangle$ | $f$ taken at $x$ |
| $F_{i-j}$ | view factor from surface $i$ to surface $j$ |
| $G$ | irradiation ($W/m^2$) |
| $h$ | heat transfer coefficient ($W/m^2$ K) |
| h | Planck's constant, $6.626 \times 10^{-34}$ (J/s) |
| $h_{cont}$ | contact coefficient ($W/m^2$ K) |
| $J$ | radiosity ($W/m^2$) |
| $k$ | thermal conductivity (W/m K) |
| $k$ | Boltzmann's constant, $1.3806 \times 10^{-23}$ (J/K) |
| $L$ | filament coil length (m) |
| $\lambda$ | wavelength (m) |
| $l_f$ | filament length (m) |
| $m$ | mass (kg) |
| $Q_c$ | conduction heat transfer rate (W) |
| $Q_{rad}$ | radiation heat transfer rate (W) |
| $q_{rad}$ | radiation heat flux ($W/m^2$) |
| $R$ | lamp resistance (Ω) |
| $r_{\lambda,i}$ | reflectivity of surface $i$ at $\lambda$ |
| $r_w$ | electric resistivity of tungsten (Ω m) |
| $\rho$ | density ($kg/m^3$) |
| $s$ | lamp spacing (m) |
| $T$ | temperature (K) |
| $t$ | time (s) |
| $\tau_{\lambda,i}$ | transmissivity of surface $i$ at $\lambda$ |
| $U$ | voltage (V) |

*Subscripts*

| | |
|---|---|
| air | cooling air |
| back | back side |
| ceram | ceramic |
| c | coil |
| f | filament |
| front | front side |
| g | protective glass |
| l | lamp glass |
| $\lambda$ | wavelength or wavelength interval |
| Ne | neon |
| quartz | quartz |
| r | reflector |
| W | tungsten |

Experiments on a small-scale heater designed for the paper industry will be used to determine model parameters and to validate the model.

## 2. The IR heater

The particular IR heater used in this study is a frame (Itronic Drying frame 5000) designed for use in the paper industry. The principles of the design are illustrated in Fig. 1. A number of high-temperature lamps are arranged in a row in front of a ceramic reflector that redirects radiation. The reflector is coated with gold to ensure a high reflectivity in the infrared range of the spectrum. Lamps and reflector are protected from dirt and dust by a protective glass made of quartz. Heater components, especially the lamp's ends, are cooled with air to ensure a long service life. Cooling air passes over the back side of the reflector, passes the lamp ends at high speed, and also cools the front side of the reflector, the lamp bodies, and the protective glass before being exhausted.

The high-temperature lamps are the core of the IR heater. Fig. 1 includes an enlargement of such a lamp. The spiral tungsten filament is heated by an electric current to high temperatures, normally above 2000 K. The filament is enclosed by a quartz envelope. The lamp is filled with an inert gas, in this case neon, to prevent oxidation of tungsten. Small amounts of halogen are also used to inhibit the evaporation of tungsten via the halogen cycle. To maintain the atmosphere inside the lamp, the electric current must be passed into the quartz tube with a special arrangement involving a molybdenum foil. The lamp ends must be cooled to temperatures lower than 350°C for the sealing to last. The lamp body can operate at temperatures up to 900°C, but for operation of the halogen cycle, no part of the lamp should be below 250°C [12]. The design of the cooling air system is thus an important and delicate task.

## 3. Experimental work

Only a small module, approximately $0.5 \times 0.2$ m with twelve 2-kW IRK halogen lamps from Philips was used in the experimental work. The design of the module was identical to industrial units. The IR module was mounted horizontally, facing an open $1 \times 1.5$-m water-cooled tray. The tray was painted inside with a mat black colour. During the measurements, water was flowing 5 cm deep through the tray. Since water

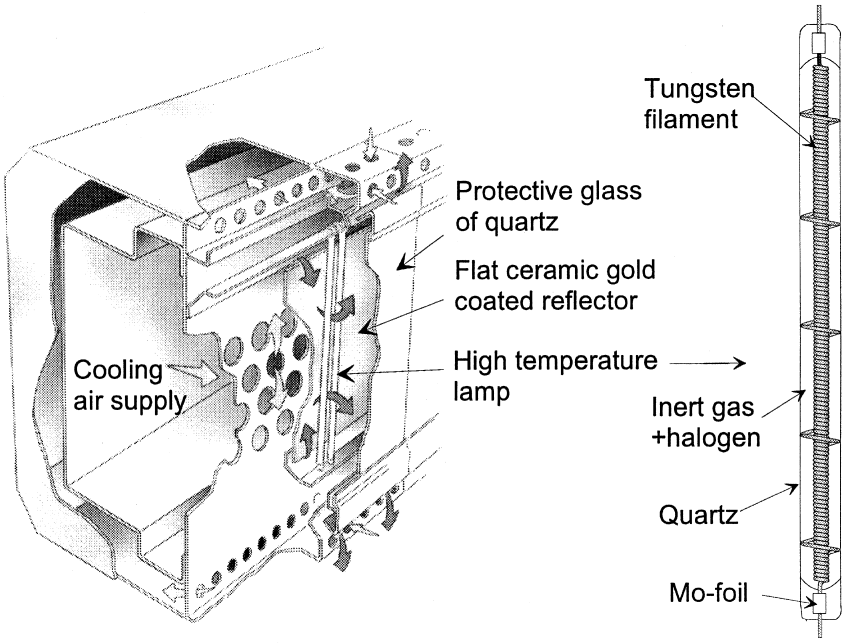


Fig. 1. IR heating frame and an enlargement of an IR lamp.

absorbs virtually all infrared radiation and the black bottom most visible radiation, the tray absorbed almost all radiation emitted from the IR heater. The set-up has been used previously to evaluate the radiation efficiency of the IR module [8].

T-type thermocouples were glued to the back side of the reflector in order to measure reflector temperature. It must be recognised that these measurements on surface temperature were uncertain due to the effects of the glue and the contact conditions between the reflector and the thermocouple. The readings should still have given an indication of the temperature within $\pm 5^{\circ}$C. Thermocouples were also inserted in the cooling air exit holes. The flow rate of cooling air was measured in the inlet using a pitot tube and evaluated to be 0.085 kg/s, i.e., 0.007 kg/s per lamp. The principle of the experimental set-up is shown in Fig. 2.

The radiation intensity in front of the heater was measured with a radiation heat flux probe, a $2\pi$-radiometer from Lands Instruments. The accuracy of the instrument is estimated by the supplier to be within $\pm 3\%$. The instrument has been described in more detail elsewhere [8]. Thermocouples and the radiometer were connected to a data acquisition system, and

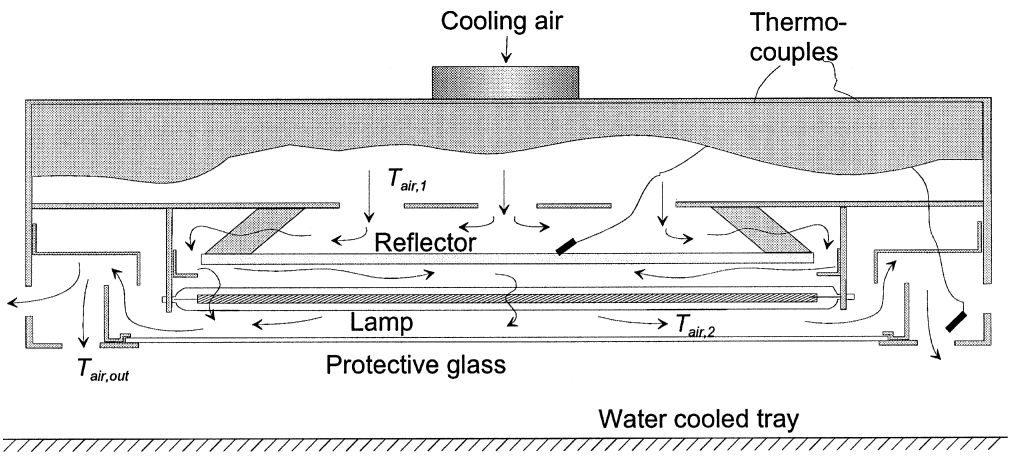


Fig. 2. View of IR heater during experiments also indicating cooling air flow.

changes during start-up and close-down of the module were logged at 1 Hz. In order to try out the dynamic response of the thermocouples, one was rapidly inserted in hot gas at steady flow and constant temperature. The dynamic response of the radiometer was evaluated in a similar way, rapidly inserting it under the IR module during steady operation. The thermocouple has a rapid response and reaches steady state within 8 s. The radiometer is slower and needs 30 s to reach a steady state value.

Electric voltage (rms) and current (rms) were measured with an Infratek Model 301A Wattmeter. The accuracy in the range of these measurements is given as $\pm 3.5\%$. There was also some noise, $\pm 2$ V and $\pm 0.2$ A, respectively, that resulted in a considerable uncertainty at low power levels. Measurements of voltage and current, together with knowledge of the module circuit, allowed the resistance of the individual lamps to be determined, which is directly dependent on filament temperature. Thus, the electric measurements provided a means to determine filament temperature. The wattmeter was also attached to a data acquisition system during some measurements, and changes were logged at 100 Hz. In these cases, data could not be logged for periods longer than 6 s.

The heater was dismounted and the dimensions of the different parts were measured using digital vernier callipers or a ruler. The resistance of the lamps (at room temperature) was measured using a multimeter. Also, one of the lamps was broken and the mass of tungsten and glass determined, as well as the dimensions of the filament. Some results from these measurements are collected in Table 1.

## 4. Mathematical model

In order to develop a mathematical description of the IR heater, the physics must be considered. A voltage is applied to the lamps and results in current and resistive losses in the filament, which will then heat up. The higher temperature will result in a higher resistivity of the filament, i.e., the lamp resistance will increase and the current and electric power will decrease. The higher temperature will also result in heat transfer from the filament to the surroundings. As the filament rapidly attains a very high temperature, most of the heat transfer will be by radiation, but some will also be transported through the lamp gas to the quartz envelope, the lamp glass, by conduction and free convection. The radiation emitted from the filament will not be affected by the neon gas in the lamp or the dry air cooling the module since these are non-participating media. The lamp glass, though very transparent, will however absorb part of the radiation, as will the protective glass and the reflector. All these components will thus heat up and are cooled with air.

Table 1
Measurements on dismounted heater and broken lamp

| Heater property | Measured value |
|---|---|
| Lamp length | 350 mm |
| Lamp spacing, $s$ | 2.5 mm |
| Lamp diameter, $d_l$ | $10.0 \pm 0.05$ mm |
| Lamp resistance (at 23°C), $R$ | $2.3 \pm 0.04$ Ω |
| Filament diameter, $d_f$ | $0.41 \pm 0.01$ mm |
| Filament coil diameter, $d_c$ | $2.89 \pm 0.01$ mm |
| Filament coil length, $L$ | $290 \pm 5$ mm |
| Mass of tungsten, $m_f$ | $11.3 \pm 0.02$ g |
| Mass of lamp glass, $m_l$ | $25.7 \pm 0.02$ g |

A cross section of the IR heater geometry is illustrated in Fig. 3. The distances indicated are small compared to the lamp length and in the centre of the heater the geometry is essentially two dimensional. Since the row of lamps is normally fairly wide, the conditions for one lamp will be quite symmetric, which results in an essentially one-dimensional geometry. Only one lamp need be considered, with a corresponding area of reflector and protective glass and a corresponding amount of cooling air. With these simplifications, the effects of lamp ends and sides will be ignored. The surroundings of the heater will be considered to be black.

### 4.1. Energy balances

#### 4.1.1. Lamp

The filament is described with a lumped heat-capacity model, Eq. (1). Due to the very large temperature change of tungsten, the temperature dependence of physical properties should be included. In the following equations, the temperature within angle brackets indicates at what temperature properties are taken.

$$\frac{\mathrm{d}}{\mathrm{d}t}\left[C_{p,\mathrm{W}}\langle T_\mathrm{f}\rangle T_\mathrm{f}\right] = \frac{1}{m_\mathrm{f}}\left[\frac{U^2}{R\langle T_\mathrm{f}\rangle} - Q_\mathrm{rad,f} - Q_\mathrm{c}\right] \tag{1}$$

The voltage, $U$, is given for the operating condition. The resistance of the filament, $R$, is proportional to the resistivity, $r_\mathrm{W}\langle T_\mathrm{f}\rangle$, as given by Eq. (2).

$$R = r_\mathrm{W}\langle T_\mathrm{f}\rangle \frac{l_\mathrm{f}}{a_\mathrm{f}} \tag{2}$$

Heat transfer by radiation, $Q_\mathrm{rad}$, must be treated for all components simultaneously and will be discussed in a subsequent section. The heat transferred by conduction/convection between the concentric cylinders — the spiral filament and the lamp glass — inside of the lamp is hard to describe accurately. The Grashof num-

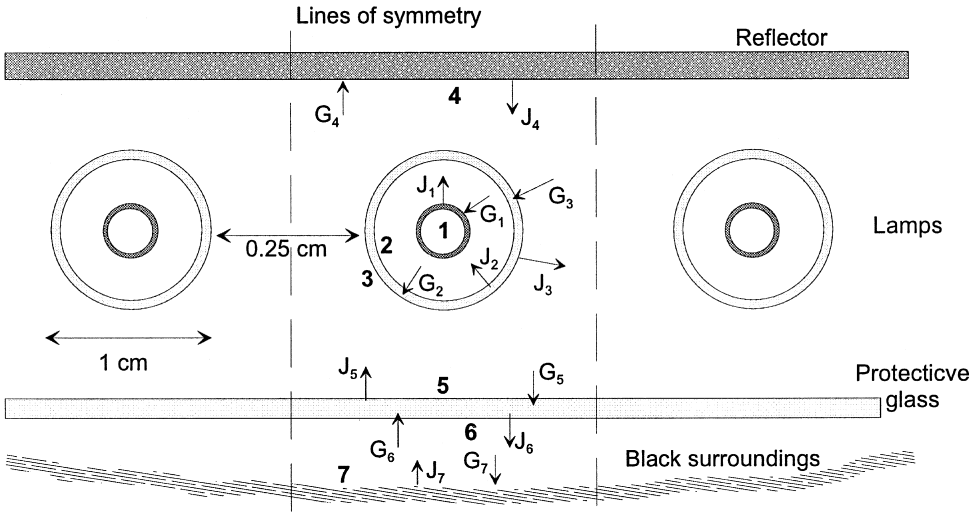


Fig. 3. Simplified view of the IR heater cross section indicating symmetry in the width and radiation flux notation.

ber, of the order 10, indicates that conduction is the dominating mechanism. A numerical study of unsteady heat conduction in the narrow gas slot in the lamp indicates that the dynamics is very fast. Steady state is reached within 0.5 s. The dynamics of this conduction is, therefore, not considered, and the heat transfer is described as steady state conduction, Eq. (3).

$$Q_c = 2\pi L k_{Ne}\left\langle\frac{T_f + T_l}{2}\right\rangle\frac{[T_f - T_l]}{\ln[d_l/d_c]} \tag{3}$$

The energy balance for the quartz glass envelope, the lamp glass, is given by Eq. (4), which includes absorbed radiation, conduction and external convection.

$$\frac{d}{dt}\left[C_{p,quartz}\langle T_l\rangle \cdot T_l\right] = \frac{1}{m_l}\left[Q_{rad,l} + Q_c - h_l A_l\left(T_l - T_{air,2}\right)\right] \tag{4}$$

*4.1.2. Reflector*

The reflector is opaque and made of ceramic with low thermal conductivity. Since the measurement available for comparison is the temperature on the back side of the reflector, it is interesting to consider the temperature difference between front side and back side. The one-dimensional heat conduction equation, Eq. (5), is used with combined radiation and convection boundary conditions at the front side and convection on the back side ($x$ is defined as increasing from the front side to the back side).

$$\frac{\partial T_r}{\partial t} = \frac{k_{ceram}}{\rho C_{p,ceram}}\frac{\partial^2 T_r}{\partial x^2}$$

$$x = \text{front} \quad k_{ceram}\frac{\partial T_r}{\partial x} = h_{r,front}\left[T_{r,front} - T_{air,2}\right] - q_{rad,r}$$

$$x = \text{back} \quad k_{ceram}\frac{\partial T_r}{\partial x} = -h_{r,back}\left[T_{r,back} - T_{air,1}\right] \tag{5}$$

*4.1.3. Protective glass*

The protective glass also absorbs some radiation and is cooled, on at least one side, with cooling air. The energy balance becomes

$$\frac{d}{dt}\left[C_{p,quartz}\langle T_g\rangle \cdot T_g\right] = \frac{1}{m_g}\left[Q_{rad,g} - h_g A_g\left[T_g - T_{air,2}\right]\right] \tag{6}$$

*4.1.4. Cooling air*

In Eqs. (4)–(6), different air temperatures are used. These temperatures are indicated in Fig. 2. No complicated model has been developed for the cooling air. The temperature is simply increased in two stages according to the energy cooled off. First, the tempera-

ture $T_{air,2}$ is calculated according to Eq. (7).

$$T_{air,2} = T_{air,1} + \frac{h_{r,back} A_r}{m_{air} C_{p,air}} \left[ T_{r,back} - T_{air,1} \right] \tag{7}$$

And finally, the outlet air temperature was calculated in a similar way according to Eq. (8).

$$T_{air,out} = T_{air,2} + \frac{h_{r,front} A_r \left[ T_{r,front} - T_{air,2} \right] + h_g A_g \left[ T_g - T_{air,2} \right] + h_l A_l \left[ T_l - T_{air,2} \right]}{m_{air} \cdot C_{p,air}} \tag{8}$$

### 4.2. Radiation heat transfer

#### 4.2.1. Radiative exchange

Radiation heat transfer without participating media in enclosures with opaque surfaces is well known and described in several textbooks, e.g., [13,14]. Examples are also given for enclosures with partially transparent windows [15], which makes the situation somewhat more complicated. The enclosure indicated between the symmetry lines in Fig. 3 is still more complicated. The filament is totally enclosed by the lamp glass, which is partially transparent. The lamp is contained between the opaque reflector and the semitransparent protective glass that obstructs the view to the surroundings. Thus, the problem is really a number of enclosures bound and connected by semitransparent walls. The treatment of this problem with the ordinary enclosure theories is not straightforward. Also, due to the simplifications, the problem is not exceedingly large, and a less elegant method can be employed without notably increasing the computational cost. Thus, the radiation heat transfer will be described in a manner similar to that suggested by Lampinen and Sievänen [16], making balances on radiosity and irradiation for all the different surfaces in the full enclosure. The same approach has been used by Ojala and Lampinen [10] and by Pettersson and Stenström [11]. Radiation will be assumed to be diffuse. Since the optical properties of the materials in the IR heater vary considerably, a reasonable model for the radiation exchange will have to be non-grey.

Radiation balances will be calculated for a number of finite wavelength intervals, i.e., a band approximation will be used. The emitted blackbody power, $E_\lambda$, in these intervals is given as the integral of Planck's law in the interval, i.e., between the wavelengths $\lambda_1$ and $\lambda_2$.

$$E_\lambda = \int_{\lambda_1}^{\lambda_2} \frac{2\pi h c_0^2}{\lambda^5 [e^{hc_0/\lambda kT} - 1]} d\lambda \tag{9}$$

The integral in Eq. (9) can be evaluated in terms of a rapidly converging infinite series [17]. The three or four first terms normally give a good result. This work has used the 10 first terms.

The simplified geometry is shown in Fig. 3. Surfaces have been assigned an index, one for opaque surfaces and one for each side of semitransparent surfaces. Radiosity, $J_i$, and irradiation, $G_i$, for each surface have been indicated with corresponding indices. The same set of radiation balance equations is used for all wavelength intervals, though the emitted power, as well as the emissivity, $\varepsilon$, the transmissivity, $\tau$, and the reflectivity, $r$, of each surface varies with wavelength. The radiosities for the different surfaces in Fig. 3 can be expressed as in Eq. (10).

$$\begin{aligned}
J_{\lambda,1} &= r_{\lambda,1} G_{\lambda,1} + \varepsilon_{\lambda,1} E_{\lambda,1} \\
J_{\lambda,2} &= r_{\lambda,2} G_{\lambda,2} + \tau_{\lambda,3} G_{\lambda,3} + \varepsilon_{\lambda,2} E_{\lambda,2} \\
J_{\lambda,3} &= r_{\lambda,3} G_{\lambda,3} + \tau_{\lambda,2} G_{\lambda,2} + \varepsilon_{\lambda,3} E_{\lambda,3} \\
J_{\lambda,4} &= r_{\lambda,4} G_{\lambda,4} + \varepsilon_{\lambda,4} E_{\lambda,4} \\
J_{\lambda,5} &= r_{\lambda,5} G_{\lambda,5} + \tau_{\lambda,6} G_{\lambda,6} + \varepsilon_{\lambda,5} E_{\lambda,5} \\
J_{\lambda,6} &= r_{\lambda,6} G_{\lambda,6} + \tau_{\lambda,5} G_{\lambda,5} + \varepsilon_{\lambda,6} E_{\lambda,6} \\
J_{\lambda,7} &= \varepsilon_{\lambda,7} E_{\lambda,7}
\end{aligned} \tag{10}$$

Note the dependence of transmissivity and irradiation on semitransparent surfaces. Note also that the assumption of a black surrounding has been inserted in the balance for surface 7. The irradiation on the different surfaces is given by Eq. (11).

$$A_i G_{\lambda,i} = \sum_j \left[ F_{j-i} A_j J_{\lambda,j} \right] \tag{11}$$

The expressions for the $G_{\lambda,i}$'s can be inserted in the expressions for the $J_{\lambda,i}$s, which, once the $E_{\lambda,i}$'s have been determined, results in a set of seven linear equations with seven unknowns. The system can be solved using, for example, Gaussian elimination. The $J_{\lambda,i}$s can then be substituted back into the relations for the $G_{\lambda,i}$s. The net heat transferred by radiation to the different sur-

faces is then determined as the sum of the net radiant flux in all wavelength intervals.

*4.2.2. View factors*

The view factors, $F_{i-j}$, used in Eq. (11) are evaluated using relations from the literature and view factor algebra. The spiral winding of the filament is so dense that it is essentially a cylinder. The view factors between infinitely long concentric cylinders are given [18] according to Eq. (12).

$$F_{1-2} = 1 \quad F_{2-1} = \frac{d_c}{d_l} \quad F_{2-2} = 1 - \frac{d_c}{d_l} \tag{12}$$

A closer inspection of the filament will, however, indicate that the 'inner cylinder' has a larger effective surface area than a smooth cylinder as shown in Fig. 4. The surface is made up of a number of small curved parts with diameter $d_f$. This increases the overall surface area with a factor of $\pi/2$. Since the actual radiating area is larger than that indicated by the diameter $d_c$, the view factor must also be increased for the reciprocity relations to be correct. Therefore, the diameter $d_c$ has been increased to $d_c \cdot \pi/2$ to reproduce an effective cylinder diameter. This is, of course, an approximate way to handle the geometrical complexity. The resulting view factors are: $F_{1-2} = 1$, $F_{2-1} = 0.454$, and $F_{2-2} = 0.546$.

Due to the symmetry in Fig. 3, each lamp can be considered with a view factor to itself that is equal to the sum of the view factors to the two adjacent lamps. The view factor between two (infinitely long) cylinders of diameter $d$ with the distance $s$ between them are given [18] according to Eq. (13).

$$F_{\text{cyl-cyl}} = \frac{1}{\pi}\left[\sqrt{\left[1+\frac{s}{d}\right]^2 - 1} + \sin^{-1}\left[\frac{1}{1+s/d}\right] - \left[1+\frac{s}{d}\right]\right] \tag{13}$$

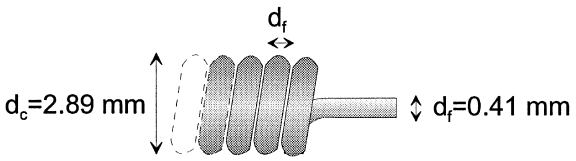


Fig. 4. Detail of filament geometry.

Since there is one cylinder on each side, the view factor is twice the result of Eq. (13), i.e., $F_{3-3} = 0.272$. Since half of the remaining radiation emitted from the lamp will hit the reflector and half the protective glass, the following view factors are determined: $F_{3-4} = F_{3-5} = 1/2(1 - F_{3-3}) = 0.365$. Reciprocity and summation relations then give: $F_{4-3} = F_{5-3} = 0.915$ and $F_{4-5} = F_{5-4} = 0.085$. The view factor from the protective glass to the surroundings is assumed to be unity. All other view factors are zero.

*4.3. Physical properties*

In Eqs. (1), (4) and (6) the specific heat of tungsten and quartz as a function of temperature is needed. Also, the temperature dependence of the resistivity of tungsten and the conductivity of neon are required. Relations for these properties are summarised in Table 2. For the specific heat, these correlations have been collected from literature [19,20] and seem to be in agreement with other available data. The resistivity and the conductivity has been fitted to data from the literature [21–24]. In both cases, the coefficient of determination is above 0.999 even though there are some minor inconsistencies in data. Note that the linear relation often used to describe the resistivity of metals is inadequate for use over such large temperature intervals as considered here. The specific heat of the reflector material is $C_{p,\text{ceram}} = 800$ (J/kg K).

The optical properties, i.e., reflectivity, emissivity, and transmissivity, of tungsten, gold, and quartz as function of wavelength are needed for evaluation of the radiation heat transfer in the IR heater. The emis-

Table 2
Temperature dependence of properties (units according to notation list)

| Property temperature dependence | Range | Source |
|---|---|---|
| $t = \frac{T}{10^3}$ $C_{p,\text{W}} = \frac{[23.9593+2.63968t+1.25775t^2-0.25364t^3-(0.048407)/t^2]}{183.84\times10^{-3}}$ | $298 < T < 1900$ | [20] |
| $t = \frac{T}{10^3}$ $C_{p,\text{W}} = \frac{[-22.5764+90.2798t-44.2715t^2+7.17663t^3-(24.0974)/t^2]}{183.84\times10^{-3}}$ | $1900 < T < 3680$ | [20] |
| $C_{p,\text{quartz}} = \frac{[55.98+15.4\times10^{-3}T-(14.4\times10^5)/T^2]}{60.085\times10^{-3}}$ | $298 < T < 1300$ | [21] |
| $r_{\text{W}} = -5.0134\times10^{-9} + 7.3070759\times10^{-11}T^{1.1796583}$ | $300 < T < 3655$ | This work |
| $k_{\text{Ne}} = -3.6018021\times10^{-3} + 1.4290623\times10^{-3}T^{0.63362378}$ | $100 < T < 2500$ | This work |

sivity of tungsten at different temperatures and short wavelengths (0.25–3 μm) is quite well explored and can be found in several sources, e.g., [21,25]. At longer wavelengths, the data becomes more scarce, represented by few wavelengths and few temperatures. In order to interpolate between the data at longer wavelengths, a three-term approximation of the Hagen–Rubens emissivity relation [25,26], Eq. (14), has been used. The agreement between the relation and data above 2.5 μm is good.

$$\varepsilon_{\lambda,1} = 0.365\left[\frac{r_W}{\lambda}\right]^{1/2} + 0.0667\left[\frac{r_W}{\lambda}\right] + 0.0061\left[\frac{r_W}{\lambda}\right]^{3/2} \quad (14)$$

The optical properties of gold and quartz have been collected from the work by Ojala and Lampinen [10,27], the data for clean parts are used in this work. Fig. 5 shows the emissivity of tungsten at three different temperatures, as well as the reflectivity of gold and the emissivity (i.e., the absorptivity) of quartz glass. In the original reference no data was given for the thickness of the quartz glass, but as it was collected from an IR heater it should be some 3–4 mm. Note that an emissivity for a glass material can only be defined if it has a uniform temperature throughout its thickness. All model equations implicitly assume a uniform temperature in all semitransparent parts which is a prerequisite for the approach to radiation heat transfer. The data for glass and gold are presented in wavelength intervals in the references and are presented in that way in Fig. 5. Thus, the graph also illustrates some of the wavelength intervals used in the numerical solution, which, however, was performed over the range 0.4–20 μm. The data for tungsten was arranged into the same bands, with the emissivity taken at the mean wavelengths. The properties for glass and gold are in rough agreement with other sources. However, the data are measured and collected at one temperature. This is a possible limitation when it comes to the lamp glass. The other parts are not heated to such an extent that the temperature dependence on the optical properties is needed.

### 4.4. Solution procedure and parameter estimation

The mathematical model described above consists of three very stiff and non-linear ordinary differential equations (ODE), (1), (4), (6), and one partial differential equation (PDE), (5), governed by changing combined radiation and convection boundary conditions. The solution of the radiation heat transfer necessitates the solution of the radiation balances for each of the 40 wavelength bands employed. These wavelength bands cover the spectral range from 0.4–20 μm. The temperature dependence of the specific heat results in a

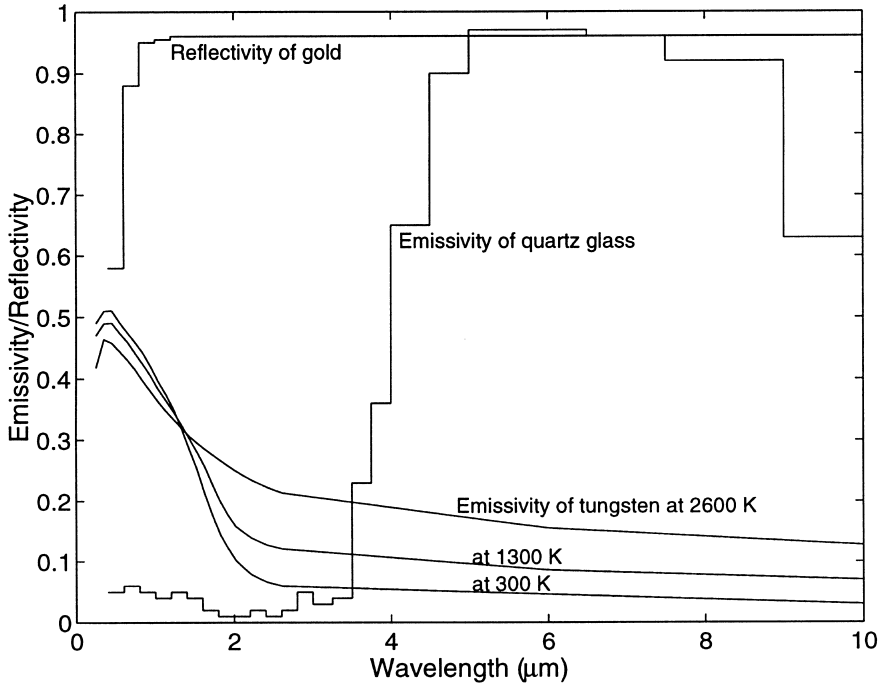


Fig. 5. Optical properties of tungsten at different temperatures, the reflectivity of gold and the emissivity of quartz (3–4 mm thick).

solution of the ODEs for the specific heat times the temperature. Since the temperature is needed in the heat transfer calculations, this adds the solution of a number of non-linear equations during each iteration. There are also a number of additional algebraic relations. The tool for solution of the model has been Matlab 5.1 [28].

The PDE, Eq. (5), underwent discretisation into a set of ODEs using a method of lines and a centred-difference approximation. The boundary conditions were introduced using the method of false boundaries [29]. The resulting ODEs are solved together with the ODEs of the model using a variable order, stiff differential equation solver in Matlab (`ode15s`) [30]. The relative error tolerance for each iteration was set to $10^{-4}$ (0.01% in each iteration) and the absolute error tolerance to $10^{-8}$. The 'linear' equation system is solved, 40 times for each iteration, using Gaussian elimination. The non-linear equations involving the specific heat are transformed into higher-order polynomial equations and solved using standard routines and a root selected as being positive and real.

The model contains four heat transfer coefficients yet to be determined, $h_{r,back}$, $h_{r,front}$, $h_g$, and $h_l$. As the flow is rather complex, there are hardly any correlations available for these heat transfer coefficients. Using engineering rules of thumb, based on flow rate and cross section of the channels, the heat transfer coefficient should be of the order of 50 W/(m$^2$ K), but a more accurate estimation must be based on the temperature measurements performed. Since only the temperature on the centre of the back reflector and the filament temperature can be considered as accurate for the model geometry, only two measurements are available. It was, therefore, decided to simplify the model somewhat. The heat transfer coefficients for all the flat surfaces was set to be equal, i.e., $h_{r,back} = h_{r,front} = h_g$. These coefficients are probably similar and will subsequently be denoted $h_r$. The heat transfer coefficient for the tube-shaped lamp, $h_l$, is probably somewhat different, but of the same order of magnitude as $h_r$.

In order to estimate the values of the two heat transfer coefficients, three different voltages (159, 249, and 393 V) were chosen, with experimental results available for both filament temperature and reflector temperature at steady state. Then, the steady state model output was compared to the experimental data while varying the heat transfer coefficients. An attempt was made to minimise the sum of the squared normalised difference between model and experiment. As it turned out, there were several local minima to this function with very similar residual error. Definite values for the best choice of heat transfer coefficients thus were not obtained. When disregarding unrealistic values for the heat transfer coefficients and values resulting in unrealistic output (e.g., lamp glass temperatures well above 1000°C) most of the minima found were in the range $h_r = 55$–$65$ W/(m$^2$ K) and $h_l = 35$–$45$ W/(m$^2$ K). It was decided to use the values $h_r = 62$ W/(m$^2$ K) and $h_l = 40$ W/(m$^2$ K) as given by one minimum. The sensitivity of these values on steady state results is illustrated in the results section below.

## 5. Results

### 5.1. Steady state

The model described above uses voltage as the only input while predicting several outputs, including temperature of filament, lamp glass, reflector, protective glass, and cooling air. Fig. 6 shows the agreement between simulated and experimental values for the filament temperature at steady state, in the range of voltages studied. Because the filament temperature is directly connected to lamp resistance, which in turn is connected to electric power, the electric power per lamp has also been plotted. Note that the voltage given is the voltage to the IR heater, not to the individual lamps. The agreement is good in the entire range of voltages; the filament temperature is predicted within 25 K (1.5%), the largest deviations being at low voltage. The sensitivity to changes in the heat transfer coefficients has also been indicated. These coefficients have a limited influence on filament temperature and thus on electric power level, as long as they are the correct order of magnitude. Another interesting result is that roughly 16% of the electric power at 400 V is transported by conduction through the lamp gas. At 130 V this lost fraction is as high as 45%. At reduced voltages, the IR lamp is not an efficient radiator. If it used a gas with lower thermal conductivity, such as argon, these losses might be reduced.

In Fig. 7 the steady state temperature on the back side of the reflector, from simulations and experiments, is shown. Though there is a spread in experimental data, the agreement with the simulation is satisfactory. The spread in data is probably due to variations in cooling air inlet temperature and flow rate. It is also possible that the contact conditions between reflector and thermocouple changed during the series of experiments. Again, the sensitivity to a 20% increase or decrease in the heat transfer coefficients has been illustrated with dotted lines. Increasing only $h_l$ decreases the reflector temperature by 0.5–2°C, and the extensive changes shown in the graph can be attributed to the change in $h_r$. The influence of the heat transfer coefficient obviously increases with increasing voltage.

The outlet air temperature was measured but not used for the estimation of the heat transfer coefficients. It was not used because in this small module the influence of side walls and ends is much larger than for a full scale heater, which adds relatively large areas to be

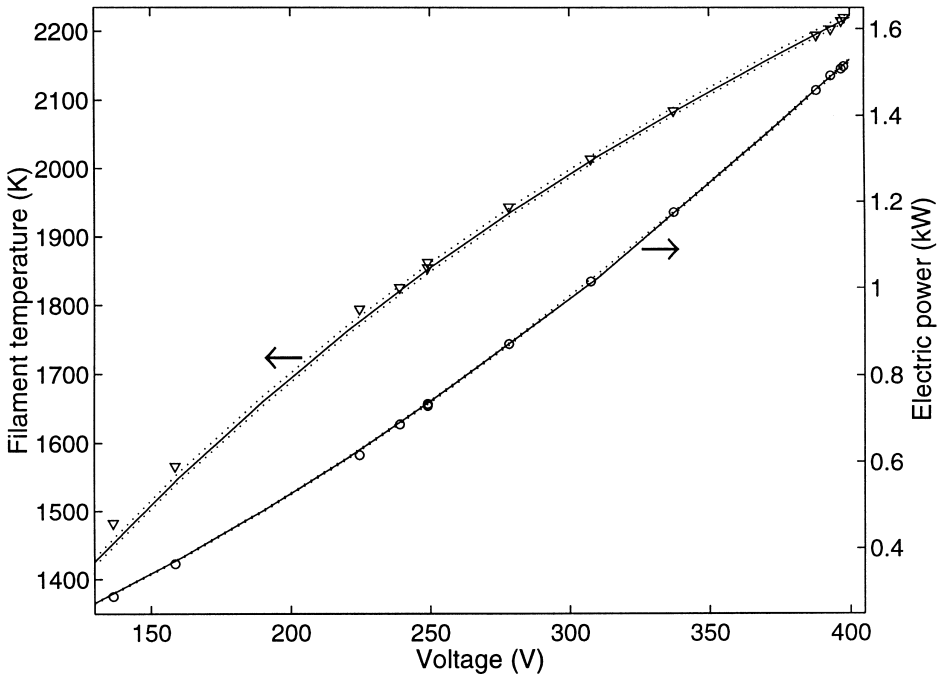


Fig. 6. Experimental and model steady state results for the filament temperature and electric power at different voltage. The influence of a 20% increase or decrease in $h_r$ and $h_l$ is indicated with dotted lines.

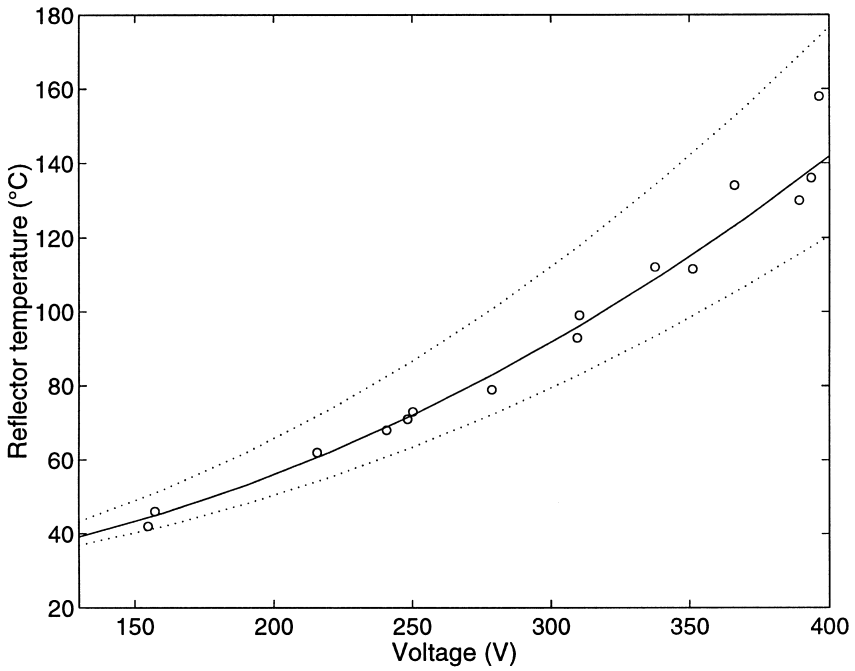


Fig. 7. Steady state temperature on the back side of the reflector as a function of voltage from experiments and model. The influence of a 20% increase or decrease in $h_r$ and $h_l$ is indicated with dotted lines.

cooled that are not included in the model. Thus, the model is not expected to give accurate predictions of the cooling air outlet temperature, but the order of magnitude should be correct. The experimental results on cooling air are generally within 5° from the model predictions though with some differences in trend.

No experimental measurements on the temperature of lamp glass and protective glass were performed. Evin [7] somehow measured the lamp glass temperature in a similar heater and indicated a temperature a little over 800°C. The temperature of the lamp glass as predicted by the model is, at high voltage, in rough agreement with this measurement.

So far, the steady state results have been compared and found to be in satisfactory agreement with experimental data. More information about the accuracy of the physical description can be obtained by comparing the dynamic response to load changes as measured on the actual heater and as predicted by the model. All comparisons below will be based on $h_r = 62$ W/(m$^2$ K) and $h_l = 40$ W/(m$^2$ K).

### 5.2. Transient conditions

The dynamics of the filament are very fast and is, in combination with the slower time response of the other components, the main reason for the numerical stiffness of the system. Fig. 8 shows the step response when increasing the voltage from 0 to 308 V, as predicted by the model and from measurements. The agreement seems to be fair. Because data could not be logged for longer than 6 s, it was not possible to follow the response all the way to steady state, about 1–2 min. The time, however, is sufficient to follow 97% of the change. From Fig. 6 it can be seen that the steady state values also are in good agreement.

Because it is not possible to measure voltage and current if the heater is turned off, the cooling down of the filament was compared when decreasing the voltage from 397 to 222 V instead. The result is indicated in Fig. 9. We can see that measured and simulated temperature is in excellent agreement at steady state. Again it is not possible to follow the response all the way to steady state, but the most important data is there, and the agreement is good. The temperature decrease is slightly faster in the measured curve, but given the noise level the difference is not very important.

In Fig. 10, the temperature on the back side of the reflector is illustrated when increasing the voltage from 0 to 249 V, and after 1000 s, back to 0 V again. The agreement is good in the heat-up as well as in the cool-down stage of the cycle. As with all components except the filament, the step response is rather slow, in the order of minutes. The cooling air temperature,

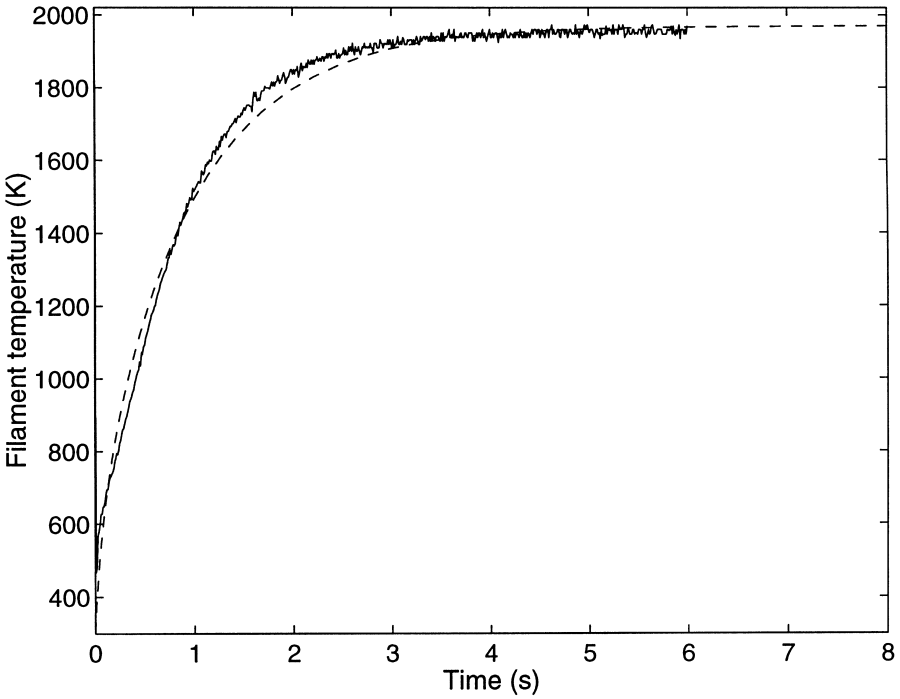


Fig. 8. Step response of filament temperature when increasing the voltage from 0 to 308 V. Solid line is measured and dashed line is simulated.

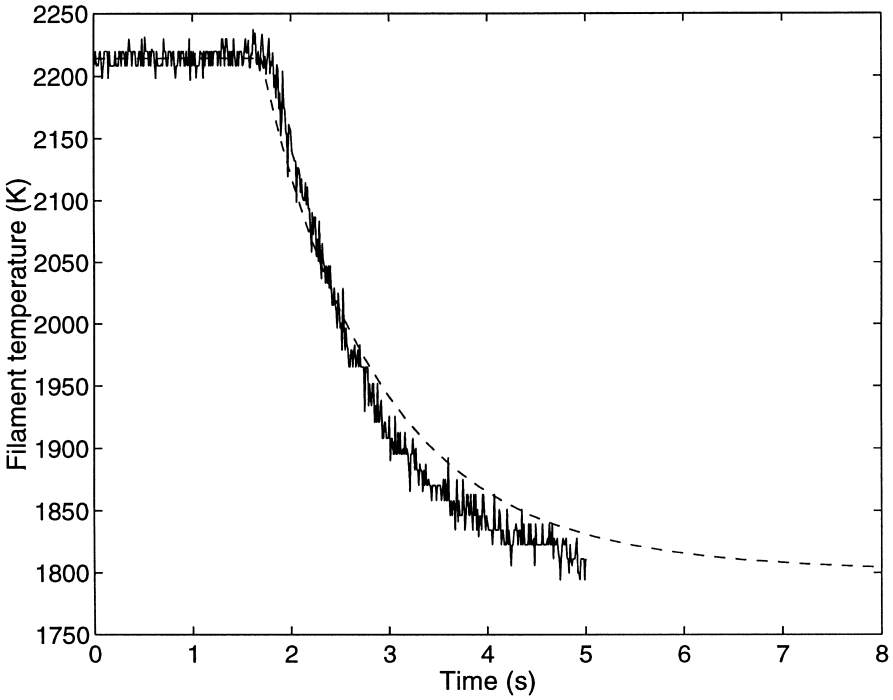


Fig. 9. Step response of filament temperature when decreasing the voltage from 397 to 222 V. Solid line is measured and dashed line is simulated.

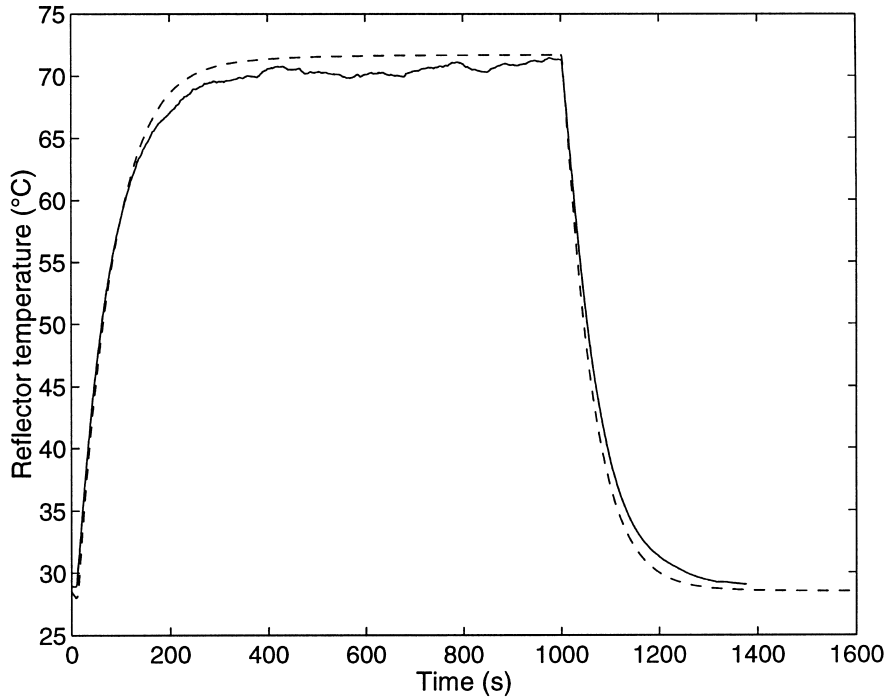


Fig. 10. Temperature on the back side of the reflector when increasing the voltage from 0 to 249 V and back to 0 V. Solid line is measured and dashed line is simulated.

though not presented here, is in equally good agreement for the same cycle.

Finally, the output of the heater, the radiation heat flux to the surroundings, is compared in Fig. 11. Since the measurement with the radiometer is the output at a specific point at a specific distance, and the model predicts the total radiation to the surroundings, the results have been normalised. The measured curve is slower to increase than the simulated curve, but when considering the time response of the radiometer the agreement is good. Both curves increase rapidly and then make a sharp bend into a much slower increase. The intensity increases rapidly, within seconds, to about 82% of the steady state result. Then it takes several minutes to actually reach the steady state output. The normalised curves are almost identical at a wide range of power levels. This illustrates that the fast dynamics of the filament results in about 82% of the final output, but the full output is not reached until the other components have reached their steady state temperatures after several minutes. Suppliers of IR heaters often talk about instant on and instant off, but that is only about 80% accurate.

## 6. Conclusions

It must be concluded that the model describes the physics of the IR heater well, with respect to steady state temperatures, as well as transient behaviour. Also, the agreement in radiation intensity is a strong argument for the proposed model. The overall physics included in the model seems to be a rather accurate description of the important phenomena. Altering only the voltage gives a good prediction of operating conditions at different power levels. Even though the heat transfer coefficients involved in the model have not been decisively determined, the magnitude is likely to be correct. The heat transfer coefficient for cooling the lamp body is especially uncertain since there are no experimental data available sensitive to this variable. Actually, this heat transfer coefficient can be varied appreciably without causing large errors in any measured temperature. Measurements on the temperature of the lamp glass and the protective glass would make important improvements in the model parameter estimation possible. Such measurements are, however, associated with large experimental problems. As it is, the model still indicates that a large fraction of the supplied electricity is lost due to conduction through the lamp gas, which is eventually cooled off by convection at the exterior of the lamp glass.

The most limiting assumption used is the geometric simplification into essentially one dimension. For large-scale applications, the assumption of symmetry

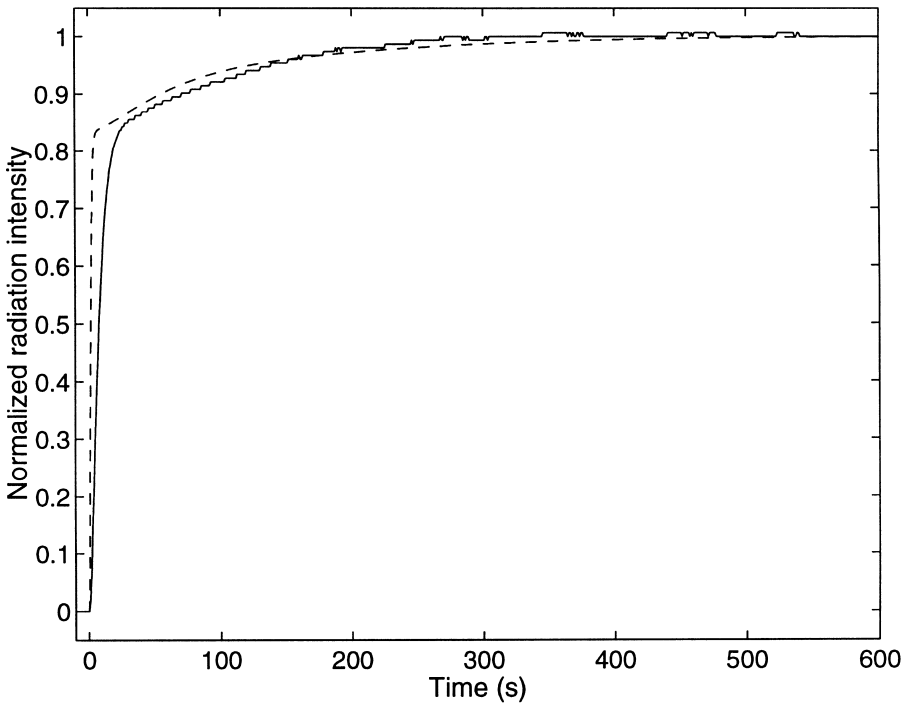


Fig. 11. Normalised step response in radiation intensity when increasing the voltage from 0 to 307 V. Solid line is measured using the radiometer and dashed line is simulated.

in the width direction is probably satisfactory, but there is no symmetry at all in the length direction. The assumption allows determination of properties in the centre of the heater, but experimental work [8] indicates that the influence of the length scale is important for the overall properties and efficiency.

## Acknowledgements

Mr. Klas-Göran Dahl, Itronic Sweden AB, is acknowledged for providing the evaluated IR heater and for sharing some of his experience and knowledge of IR heaters. Mr. Aleksander Burno and Mr. Tommy Andersson are acknowledged for their assistance with part of the experimental work. Sydkraft and SGC are acknowledged for financial support.

## References

[1] S.B. Sathe, R.E. Peck, T.W. Tong, A numerical analysis of heat transfer and combustion in porous radiant burners, International Journal of Heat and Mass Transfer 33 (1990) 1331–1338.
[2] K. Hanamura, R. Echigo, An analysis of flame stabilization mechanism in radiation burners, Wärme- und Stoffübertragung 26 (1991) 377–383.
[3] P.H. Bouma, L.M.T. Somers, L.P.H. de Goey, J.K. Nieuwenhuizen, Modelling of methane–air combustion on ceramic foam surface burners in the radiation mode, Heat and Technology 13 (2) (1995) 127–140.
[4] R.F. Speyer, W.-Y. Lin, G. Agarwal, Radiant efficiencies and performance considerations of commercially manufactured gas radiant burners, Experimental Heat Transfer 9 (1996) 213–245.
[5] R. Mital, J.P. Gore, R. Viskanta, S. Singh, Radiation efficiency and structure of flames stabilized inside radiant porous ceramic burners, National Heat Transfer Conference (ASME) 6 (1996) 131–137.
[6] N. Bédard, S. Brunet, Évaluation d'émetteurs infrarouges électriques et de radiants à gaz, in: UIE XIII Congress on Electricity Applications, 1996, pp. FIN27–FIN36.
[7] F. Evin, H. Junginger, P. le Peurian, Sunair Le, Un nouveau mode de séchage du papier utilisant les rayonnements IR électriques, in: UIE XIII Congress on Electricity Applications, 1996, pp. FIN69–FIN76.
[8] M. Pettersson, S. Stenström, Experimental evaluation of electric infrared dryers, TAPPI Journal (accepted).
[9] K.T. Ojala, Studies on infrared drying of paper, use of integrating spheres in FTIR-measurements, and heat and mass transfer inside paper, Ph.D. thesis, Helsinki University of Technology, 1993.
[10] K.T. Ojala, M.J. Lampinen, Modeling, measurements and efficiencies of infrared dryers for paper drying, in: A.S. Mujumdar (Ed.), Handbook of Industrial Drying, 2nd ed., Marcel Dekker, New York, 1995, pp. 931–976.
[11] M. Pettersson, S. Stenström, Absorption of infrared radiation and the radiation transfer mechanism in paper. Part II: application to infrared dryers, Journal of Pulp and Paper Science 24 (11) (1998) 356–363.
[12] Philips Lighting, Engineering and design, (Information Material from Philips Lighting), Printed in the Netherlands, 1990.
[13] M.F. Modest, in: Radiative Heat Transfer, McGraw-Hill, New York, 1993, pp. 193–294.
[14] R. Siegel, J.R. Howell, in: Thermal Radiation Heat Transfer, 3rd ed., Hemisphere, Washington, DC, 1992, pp. 253–414.
[15] R. Siegel, J.R. Howell, in: Thermal Radiation Heat Transfer, 3rd ed., Hemisphere, Washington, DC, 1992, pp. 936–939.
[16] M.J. Lampinen, M. Sievänen, An analysis of the efficiency of a radiative dryer, in: Proceedings of the Sixth International Drying Symposium (IDS '88) Versailles, 1988, pp. 195–202.
[17] R. Siegel, J.R. Howell, in: Thermal Radiation Heat Transfer, 3rd ed., Hemisphere, Washington, DC, 1992, pp. 31–33.
[18] R. Siegel, J.R. Howell, in: Thermal Radiation Heat Transfer, 3rd ed., Hemisphere, Washington, DC, 1992, pp. 1027–1037.
[19] Domalsi and hearing, condensed phase heat capacity data, in: W.G. Mallard, P.J. Linstrom (Eds.), NIST Chemistry WebBook, NIST Standard Reference Database Number 69, National Institute of Standards and Technology, Gaithersburg, MD 20899, March 1998, http:\webbook.nist.gov.
[20] N.P. Bansal, R.H. Doremus, Handbook of Glass Properties, Academic Press, New York, 1986, p. 10.
[21] D.R. Lide (Ed.), CRC Handbook of Chemistry and Physics, 73rd ed., CRC Press, Boca Raton, 1992, pp. 10-305–10-306.
[22] D.R. Lide (Ed.), CRC Handbook of Chemistry and Physics, 73rd ed., CRC Press, Boca Raton, 1992, pp. 6–172.
[23] VDI-Wärmeatlas: Berechnungsblätter für den Wärmeübertragung, 7th ed., VDI Verlag, Düsseldorf, 1994, p. Dc 27.
[24] B. Elvers, S. Hawkins, G. Schulz (eds.), Ullman's Encyclopedia of Industrial Chemistry, 5th ed., vol. A 17, Verlag Chemie, Weinheim, 1991, p. 492.
[25] E.A. Brandes, G.B. Brook, Smithells Metals Reference Book, 7th ed., Butterworth–Heinemann, London, 1992, pp. 17-1–17-11.
[26] R. Siegel, J.R. Howell, in: Thermal Radiation Heat Transfer, 3rd ed., Hemisphere, Washington, DC, 1992, p. 123.
[27] M.J. Lampinen, K.T. Ojala, E. Koski, Modeling and measurements of infrared dryers for coated paper, Drying Technology 9 (4) (1991) 973–1017.
[28] MATLAB, Using Matlab, version 5, MathWorks, 1996.
[29] M.E. Davis, Numerical Methods and Modelling for Chemical Engineers, Wiley, New York, 1984, pp. 67–75–128–147.
[30] L.F. Shampine, M.W. Reichelt, The Matlab ODE suite, SIAM Journal of Sci. Comput 18 (1) (1997) 1–22.